Abstract The interaction of light with nanostructured materials provides exciting new opportunities for investigating classical wave analogies of quantum phenomena. A topic of particular interest forms the interplay between wave physics and chaos in systems where a small perturbation can drive the behavior from the classical to chaotic regime. Here, we report an all-optical laser-driven transition from order to chaos in integrated chips on a silicon photonics platform. A square photonic crystal microcavity at telecom wavelengths is tuned from an ordered into a chaotic regime through a perturbation induced by ultrafast laser pulses in the ultraviolet range. The chaotic dynamics of weak probe pulses in the near infrared is characterized for different pump-probe delay times and at various positions in the cavity, with high spatial accuracy. Our experimental analysis, confirmed by numerical modelling based on random matrices, demonstrates that nonlinear optics can be used to control reversibly the chaotic behavior of light in optical resonators.

Ultrafast all-optical order-to-chaos transition in silicon photonic crystal chips

Roman Bruck[1,†], Changxu Liu[2,†], Otto L. Muskens[1], Andrea Fratalocchi[2], and Andrea Di Falco[3,*]

1. Introduction

Deterministic chaos is characterized by exponential sensitivity to the initial conditions and is an ubiquitous phenomenon observed in different systems, including laser diodes, electronic circuits, fluids, chemical reactions, brains and beyond [1–6]. The dynamics of the order-to-chaos transition in physical systems has been studied in a variety of platforms [3, 7–12] and is of substantial importance, both for fundamental physics and practical applications including secure communication [13], random number generation [14], data storage [15, 16], random lasers [17] and energy harvesting [18, 19]. The transition from ordered to chaotic regimes is of particular relevance in the investigation of quantum chaos, which explores the relationship between quantum mechanics and classical chaos. Although there are many theoretical studies in the quantum order-to-chaos transition [4, 15, 20–23], experimental demonstrations are hampered by the difficulty to control accurately the system parameters and are limited to a few examples, e.g. in rotational nuclei, intense laser beams and mesoscopic electron devices [24–26].

The isomorphisms between Schrödinger and Maxwell equations allows to investigate quantum phenomena using classical waves. In this context, classical waves such as light or sound form a versatile playground for investigating effects of quantum transport, including long-range correlations and Anderson localization [27]. Classical waves can be studied in simple and compact systems that show order-to-chaos transitions and thus give further insight to such transitions in the quantum regime [28].

Here, we experimentally demonstrate ultrafast order-to-chaos transitions in an integrated photonic system comprised of a square optical resonator based on silicon-on-insulator (SOI) photonic crystal cavities (PCCs). These PCCs have been intensively studied and show a classical mode spectrum under normal conditions [18]. However, similar to classically chaotic billiards, the behaviour of these dielectric optical microresonators is very sensitive to small perturbations in the system. Using a focused femtosecond laser, we produce such perturbations via local photoexcitation inside the cavity, effectively tuning the classical system toward chaotic characteristics. The strength of this transition can be controlled by the strength of the ultrafast perturbation, its position inside the cavity, and the relative time delay between excitation and interrogation of the switched cavity. Simultaneously, the photomodulation technique can be used to spatially map the modes in the cavity [29]. Based on this all-optical setup, we demonstrate ultrafast order-to-chaos transitions in the photonic chip by dynamically manipulating laser pulses, opening a new avenue to study the quantum chaos quantitatively. These transitions are quantified by the spectral rigidity that gradually switches from a quasi-integrable to chaotic behavior and a good match with random matrix theory (RMT) simulations.

2. Setup and materials

To introduce a local perturbation to the cavity we employ the technique of ultrafast photomodulation spectroscopy (UPMS) [29, 30]. UPMS relies on ultrafast (150 fs), 400 nm wavelength laser pulses which are focused onto the surface

[1] Physics and Astronomy, Faculty of Physical Sciences and Engineering, University of Southampton, Southampton SO17 1BJ, UK [2] PRIMALIGHT, Faculty of Electrical Engineering; Applied Mathematics and Computational Science, King Abdullah University of Science and Technology (KAUST), Thuwal 23955-6900, Saudi Arabia [3] SUPA, School of Physics and Astronomy, University of St Andrews, North Haugh, St Andrews KY16 9SS, UK
†These authors contributed equally to this work.
* Corresponding author: e-mail: adf10@st-andrews.ac.uk

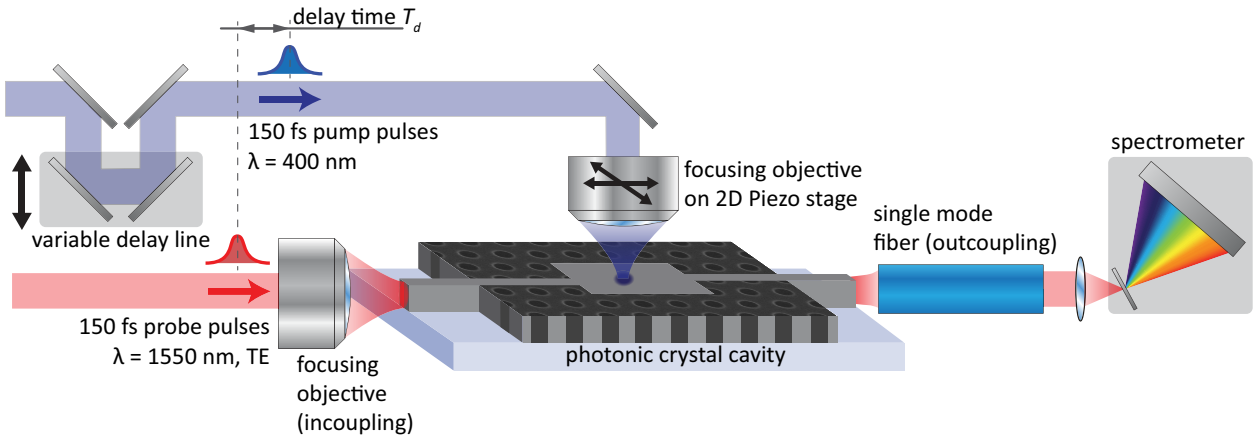

Figure 1 Experimental setup. The transmission of TE-polarized 150 fs probe pulses with a central wavelength of 1550 nm propagating through the silicon-based photonic crystal waveguides and cavity is monitored and spectrally resolved in a spectrometer. Simultaneously, 400 nm pump pulses are focused onto the cavity from the top, decreasing the refractive index of silicon in a roughly 2 µm diameter spot by plasma dispersion. The position of this perturbation and its timing with respect to the probe pulses can be freely chosen.

of the integrated photonic device to excite free carriers in silicon, lowering the refractive index locally through plasma dispersion. The employed pump fluence of approximately 72 pJ/µm^2 results in an average change of the refractive index of silicon of $\Delta n_{Si} = -0.3 + 0.04\mathrm{i}$ in the area of the pump spot [29]. Simultaneously, the transmission of infrared probe pulses through the device is monitored using a high-resolution (0.12 nm) spectrometer, as depicted in Fig. 1. The transmission spectra of the probe pulses can be analyzed as a function of the position of the pump spot on the sample and of the delay time between pump and probe pulses. The microscope objective (0.5 numerical aperture) focusing the pump light onto the sample surface was mounted on a closed-loop 2D piezo-stage, which allows us to address any position around the cavity repeatedly, with better than 100 nm accuracy.

The PCC sample was realized on a 220 nm-thick SOI substrate with a standard lithographic approach. A commercially available positive tone resist (ZEP 520A) was spun on the sample and exposed at 30 KV with a Raith Eline electron beam lithographic system. The design, consisting in a uniform, non-patterened area of 20 µm × 20 µm surrounded by a photonic crystal (lattice constant $a = 420$ nm and radius $r = 0.28a$) and access waveguides, was transferred into the silicon layer by reactive ion etching with a 50:50 mixture of SF_6 and CHF_3. The photonic crystal waveguides for in- and outcoupling were created by omitting one row in the photonic crystal (see Fig. 2a). The input waveguide is offset by 2 µm with respect to the cavity centre to excite a wide mode spectrum.

3. Experimental results

3.1. Spatial mode maps and ultrafast perturbation of cavity

The mode structure of the cavity and its sensitivity to local perturbations was analyzed by measuring spatial photomodulation maps for each wavelength. Figure 2b presents transmission spectra of the unperturbed cavity (blue curves) and for a perturbation positioned at selected points of interest (POIs) inside the cavity POI 1 – POI 4 (red curves). To rule out long-term drift of the probe laser over the duration of the spatial scan (several hours), an unperturbed reference spectrum was taken for each position. Compared to the unperturbed spectra, the spectra in presence of the perturbation show pronounced uncorrelated changes in both amplitude and spectral positions of modes, indicating a significant restructuring of the mode spectrum rather than an average spectral shift or absorption effect [31]. Typical experimental photomodulation maps are presented in Figs. 2c-e for selected wavelengths, where we plot the normalized change in transmission, $\Delta T/T$ to divide out fluctuations of the laser intensity. These photomodulation maps were obtained for a delay time of 50 ps, meaning that the pump pulses excite the cavity 50 ps before the arrival of the probe pulses. At these delay times the dynamics of the perturbation is slow compared to the typical dwell times of the modes (i.e. adiabatic regime). The photomodulation maps represent the sensitivity of the selected spectral mode to a local perturbation, and hence are related to the local field distribution of the mode inside the structure similar to other methods of perturbation using e.g. a near-field tip [32]. The maps show complex distribution patterns of high and low values inside the cavity that decay rapidly beyond the physical dimensions of the cavity (given by the dashed squares in the figures) and into the photonic crystal sidewalls. Positive modulation values (red) indicate that the transmission at the output is increased by pumping at this specific location, while negative values (blue) signify a reduced intensity.

The photomodulation maps strongly depend on the wavelength and exhibit various different forms of structuring. A full spectral evolution of the mode maps is presented as an animation in the Supporting Information. It can be observed from this animation that these structures appear and disappear uniformly over the entire cavity, demonstrating

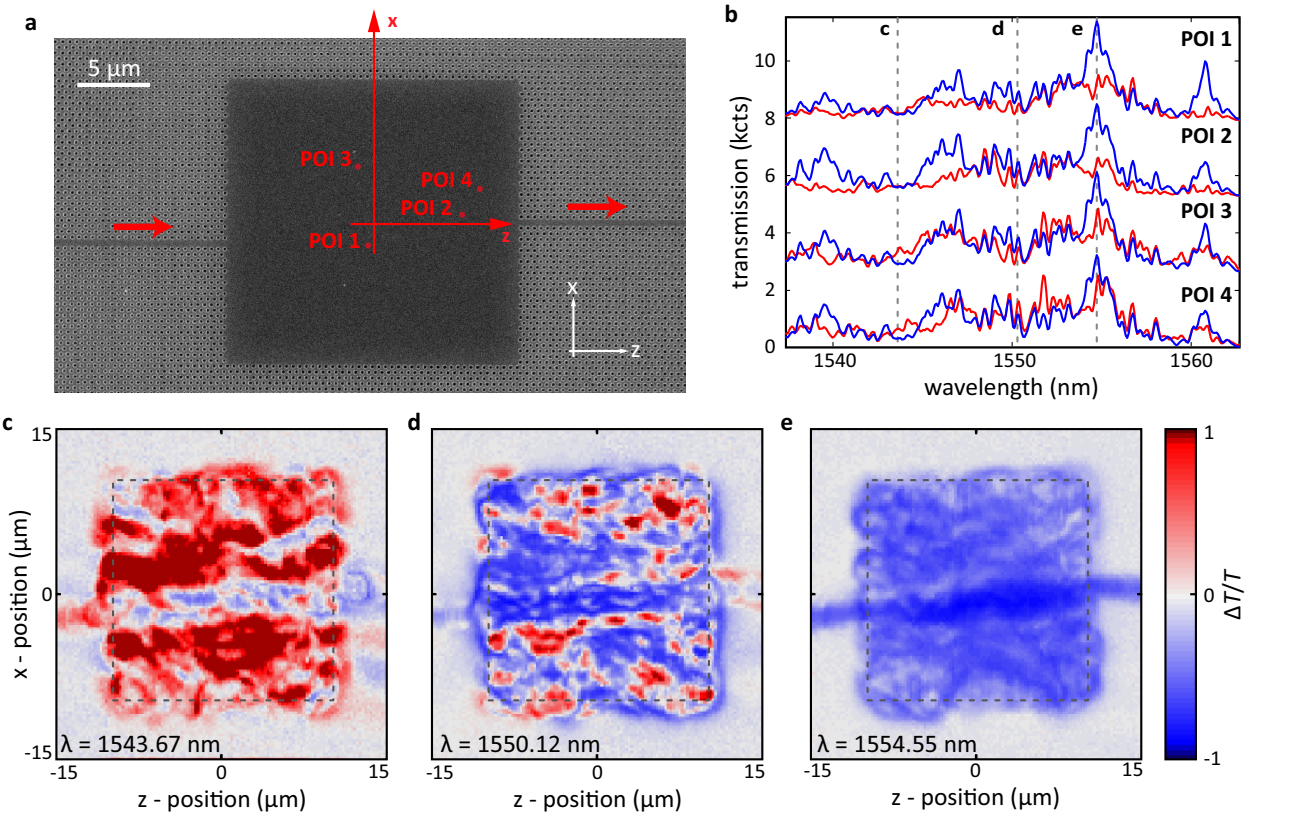

Figure 2 a) SEM micrograph of the silicon photonic crystal cavity, also showing the photonic crystal defect waveguides for in- and outcoupling. Positions of the selected POIs are shown corresponding to POI 1 X=-2 μm, Z=-0.5 μm; POI 2 X=0.5 μm, Z=6.0 μm; POI 3 X=3.75 μm, Z=-1.25 μm; POI 4 X=2.25 μm, Z=7.25 μm. b) Spectra taken at POI 1 – POI 4 for unperturbed (blue) and perturbed (red) cavity, at 50 ps delay time. c-e) Selected photomodulation maps at 50 ps delay time, giving the change in transmission depending on the position of the pump spot at wavelengths corresponding to the labels in b. An animated map showing spectral evolution is available as supplementary material.

that they correspond to well defined, individual modes of the system [33]. Many of the maps contain rapidly varying patterns with roughly equal areas of red and blue intensity, as shown in Fig. 2c, which corresponds to a position in the spectrum with a number of closely spaced modes of roughly equal transmission. Here, the effect of the perturbation on the associated modes depends strongly on the position in the cavity. At some wavelengths, the transmission is uniformly increased (Fig. 2c) or reduced (Fig. 2e). These maps are correlated with regions of respectively low and high transmission in the unperturbed spectrum, where the perturbation strongly enhances or suppresses a particular mode.

To quantify the average sensitivity of areas in the cavity to the perturbation, we define a local 'activity' parameter as the average change in transmission integrated over the investigated spectral window. The activity can be separated into the signed activity A_s, which is the average of $\Delta T/T$, and the absolute activity A_a, as the average of $|\Delta T/T|$. The signed and absolute activity maps are presented in Figs. 3a,b, with horizontal and vertical averages plotted in Fig. 3c and Figs. 3d,e respectively. The dominant feature in the signed activity map in Fig. 3a is a track of negative $\Delta T/T$ between the input and the output waveguide. This track can be observed as well in most of the individual maps and resembles a particle-like trajectory in the system [34]. We attribute the strong presence of this track in the photomodulation activity map to an perturbation-induced suppression of this direct pathway between input and output waveguides and hence an increased coupling of light into the bulk of the cavity. Enhanced coupling to long propagation paths in the cavity generally results in lower transmission due to an increased susceptibility to losses from absorption in the silicon, from reflections on the photonic crystal sidewalls, and reflections back into the input waveguide.

The blue track in the signed activity map is surrounded on both sides by red bands, indicating an overall increase in transmission. A net increase in transmission can be achieved through perturbation-induced coupling to high-transmission modes, in this case most likely as a result of near-forward scattering of light at the fringes of the central track into the exit waveguide. In the areas above and below these tracks, the contributions from the individual wavelengths tend to cancel in the signed activity map with only a small residual negative contribution of a few percent due to induced absorption and scattering losses. However, the absolute activity A_a in Fig. 3e shows average values above 0.2 over the entire

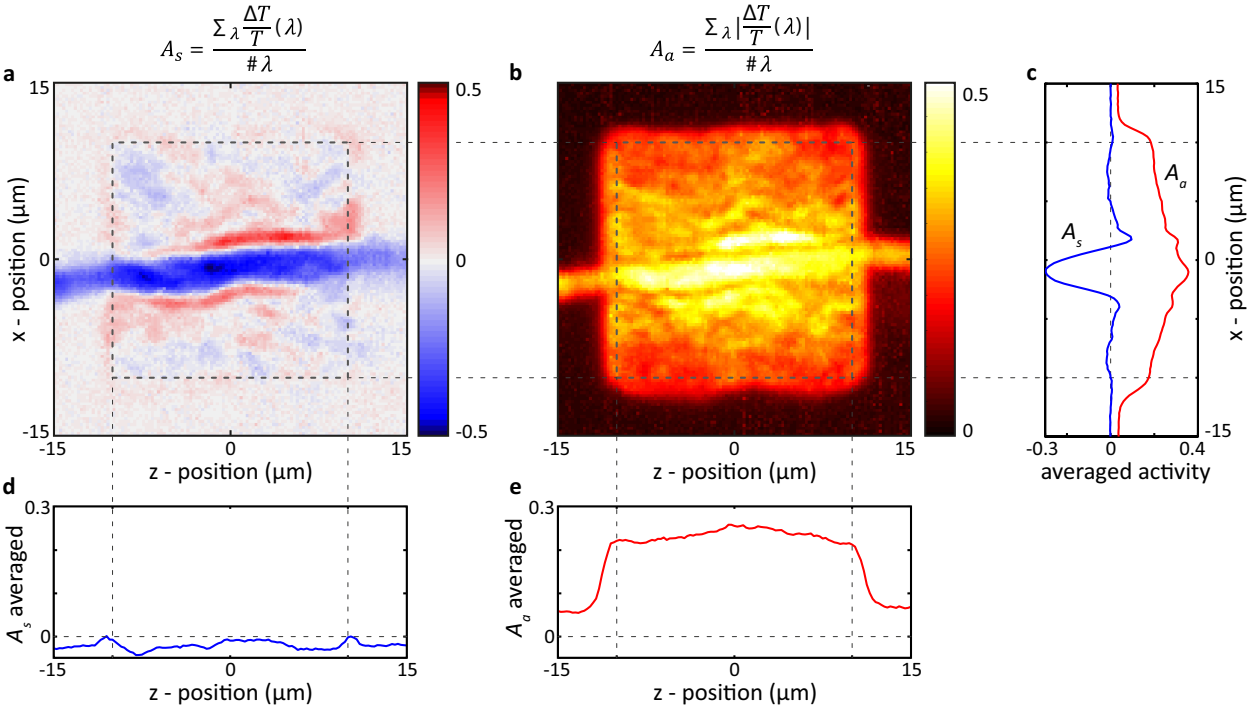

Figure 3 a) Activity map of the photonic crystal cavity at 50 ps delay time, created by averaging 512 photomodulation maps of different wavelengths (see Figs. 2b-e for examples) in the wavelength range from 1529.41 nm to 1570.58 nm. b) Absolute value activity map, based on the same dataset as a, however created by averaging the absolute value of the photomodulation maps. c-e) Horizontal (c) and vertical (d,e) averages for the signed activity As (blue lines) and the absolute value activity A_a (red lines).

cavity, indicating that the mode spectrum is significantly perturbed without causing strong changes in the average transmitted intensity. The low residual signed activity confirms that the induced perturbation is mainly stemming from changes in the real part of refractive index and not in the imaginary part (absorption) as expected given the estimated value for Δn_{Si}.

3.2. Quantifying the order-to-chaos transition

To perform an in-depth analysis on the effects of the induced perturbation on the PCC behaviour we investigate the spectral statistics of the transmission. Generally, there are two fluctuation measures that are widely used in the spectrum analysis initiated by Dyson and Mehta [35]: the level spacing distribution and the spectral rigidity (Δ_3 statistics). For our studies we apply the spectral rigidity instead on relying on level spacing distribution in the empirical spectrum analysis, because it provides information on the correlation at long ranges, not only at nearest neighbors. We started with a multiscale wavelet analysis to reconstruction the measured spectra, which provides an excellent match even when resonances overlap [36]. The wavelet analysis fits the spectrum with the sum of a series of proper wavelet functions, providing the positions of the resonant modes of the cavity (E_m). Figure 4a displays a typical experimental power density spectrum of the transmitted light and its reconstruction. The vertical green lines below the spectrum

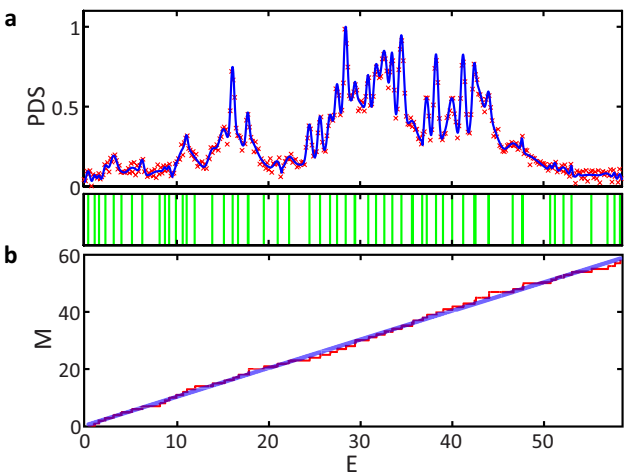

Figure 4 a) Experimental spectrum (crosses) and theoretical reconstruction via wavelet multi-scale analysis (solid line). The inset below the graph shows the positions of resonances from the reconstruction as green lines. The spectrum is unfolded so the eigenvalues are dimensionless with an average level spacing equal to unity. b) Staircase function (red) generated from the position of the resonances and its linear fit (blue).

give the positions E_m of the resonances, as extracted from the reconstruction. From these resonance positions, we generate a staircase function $M(E)$ (see Figure 4b) that counts the number of resonances below energy E. We define the

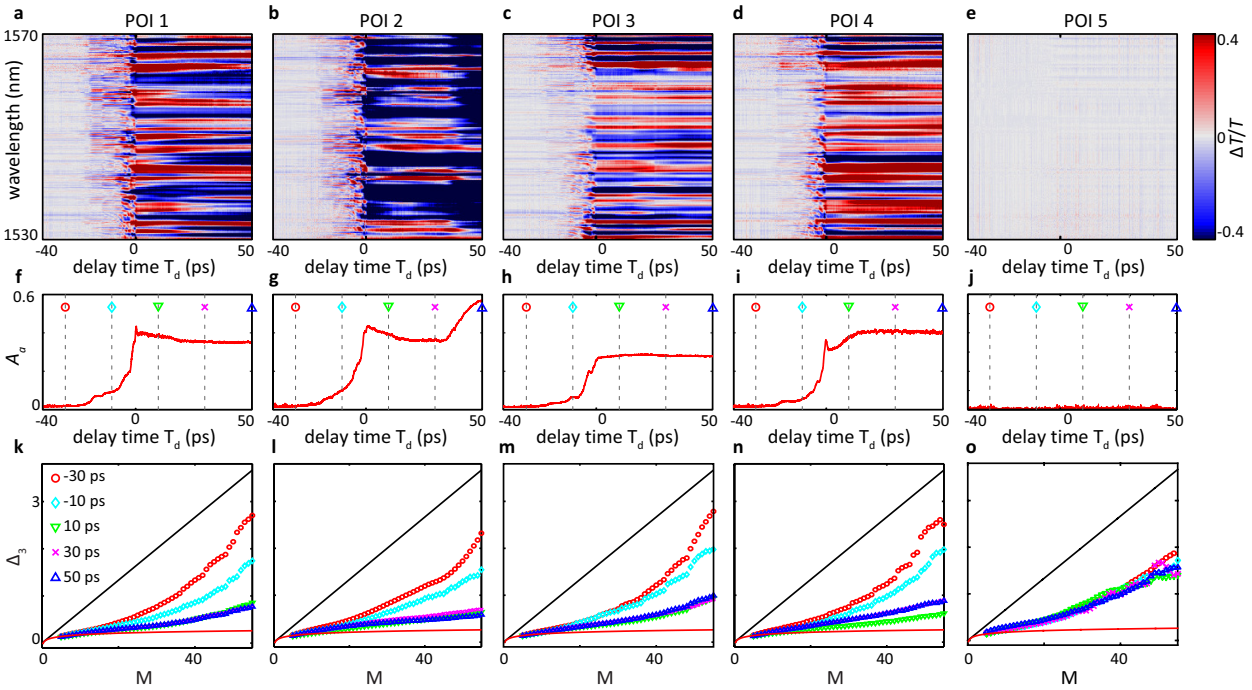

Figure 5 Δ_3 statistics. a-e, $\Delta T/T$ spectra versus delay time for the selected POIs. f-l, Absolute value activity traces of the spectra. m-q, The Δ_3 statistics of the five POIs calculated from the presented $\Delta T/T$ spectra at different delay times, as indicated by the dashed lines in f-l.

staircase function as:

$$M(E) = \int_{-\infty}^{E} dE' \sum_m \delta(E' - E_m) \qquad (1)$$

where δ is the delta function. To investigate the spectral correlation, we analyze the experimental data by the Δ_3 statistic, which is defined as

$$\Delta_3(L) = \min_{a,b} \frac{1}{L} \left\langle \int_{E_0}^{E_0+L} [M(E) - a \cdot E - b]^2 dE \right\rangle \qquad (2)$$

where L is the energy interval under consideration and the angular brackets indicate the average over E_0. It is convenient to normalize the energy E to the spacing ΔE between two adjacent energy levels. Consequently, the number of states M and the statistics Δ_3 are dimensionless quantities. The Δ_3 statistic provides a measure of the spectral rigidity, corresponding to the degree of disorder in the system. For a fixed L, the closer the staircase is to a perfectly linear curve $a \cdot E + b$, the smaller the Δ_3, and the stronger the degree of chaos as the result of the long range correlations among the resonances.

3.3. Spectral rigidity analysis for selected POIs vs delay time

We evaluated the Δ_3 statistics at the four selected POI 1 – POI 4 as well as for a pump position outside the cavity (POI5). For each point, 100 spectra were fitted and their respective Δ_3 statistics were averaged, a procedure which significantly reduces any contribution of laser fluctuations to the spectral statistics, allowing a clear and unequivocal study of sample-induced effects. Measurements were taken at different pump-probe delay times, yielding information on the relative timing of the perturbation on the mode spectrum. Figures 5a-e show the corresponding $\Delta T/T$ spectra for delay times, T_d, between -40 ps to 50 ps, together with absolute value activities shown in Figs. 5f-j. The corresponding Δ_3 statistics for five selected delay times are shown in Figs. 5k-o. When the pump pulse arrives long after the probe beam (long negative delay times), the contribution from the refractive index perturbation diminishes as most probe light has left the cavity before the arrival of the pump pulse. Thus, A_a approaches zero and the statistics at -30 ps corresponds to that of the unperturbed cavity (POI5). When the negative delay time becomes of the order of the average photon lifetime in the cavity, the induced perturbation starts affecting the probe light remaining in the cavity. As a consequence, the activities for the POIs inside the cavity start increasing from their background level at around -20 ps, which is also reflected in reduced Δ_3-values at -10 ps, pushing their curves (cyan diamonds) in Figs. 5k-o towards a more chaotic state. As expected, pumping at POI5 outside the cavity does not produce any change in the transmitted spectra, independently of the delay, and also does not influence its Δ_3 statistic.

Fully ordered systems can be described as Poisson processes with uncorrelated nearest neighbours, and exhibit a characteristic linear relationship between Δ_3 and M, as

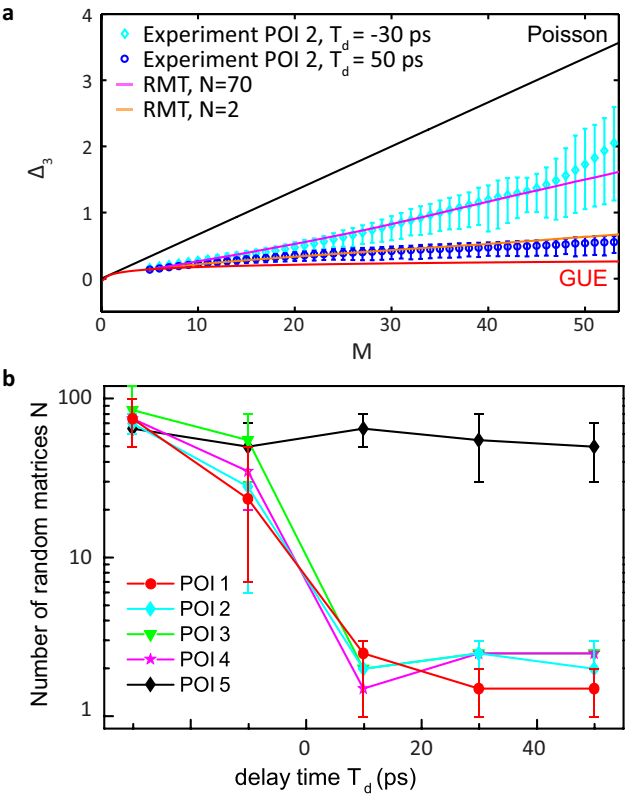

Figure 6 a) Experimental Δ_3 statistics for POI2 ($T_d = -30$ ps and 50 ps), together with theoretical model calculations for classical cavity (Poisson) and fully chaotic cavity (GUE), and random matrix theory calculations assuming N independent GUEs, with $N = 70$ (magenta) and $N = 2$ (orange). b) Fitted values for the number of GUEs N against delay time T_d for POI 1 – POI 5, showing transition from classical (uncorrelated) statistics for negative T_d to highly chaotic statistics for positive T_d.

shown with a black lines in Fig. 5k-o). Chaotic systems are instead described by the properties of Gaussian unitary ensembles (GUE) of random matrices, for which Δ_3 grows logarithmically with M, as shown by the red curves in the same figures [37]. The experimental data lie in between these limits. In order to get a quantitative and self-consistent evaluation of the degree of chaos in the experimental system before and after pumping, we employ an independent analysis based on random matrix theory (RMT) as illustrated in Fig. 6a. We start with a diagonal block matrix A composed of N uncorrelated equal-sized GUEs along the diagonal. The size of the matrix is large enough so that the analysis is independent of its size. When $N = 1$, the matrix is a GUE with correspondingly suppressed values of Δ_3 given by the logarithmic GUE statistics (red curves in Fig. 6a).

As N increases gradually, the eigenvalues of A become more uncorrelated resulting in an increment of the Δ_3 values approaching the non-chaotic regime given by Poissonian statistics (black curve in Fig. 6a). To complete the self-consistent evaluation of the disorder, we fit our experimental Δ_3 values with the RMT prediction, as shown by the magenta and orange curves in Fig. 6a for the case of POI2 at $T_d = -30$ ps and 50 ps. The experimental data and RMT prediction match well for corresponding N of 70 ± 20 and 2 ± 0.3, confirming the induction of strongly chaotic behaviour in the cavity by the perturbations. Similar values are found for the other POIs as shown in Fig. 6b.

Thus, the spectral rigidities at $T_d = -30$ ps and for the unperturbed cavity are characterized by a large number of uncorrelated channels, yielding results close to a Poisson process characteristic for non-chaotic systems. We attribute deviations from the Poisson statistic in these cases to the residual presence of chaotic fluctuations in the laser system and the actual limited number of physical modes in our system. For positive delay times, the system saturates in a strongly chaotic regime close to a GUE. The behaviour of the Δ_3 statistics is insensitive to the position of the pump pulse and strong chaotic behaviour could be induced at all investigated positions. The injected probe beam is scattered at the perturbation, effectively modifying the system toward a Sinai billiard. The relative insensitivity on position is consistent with the dynamics of the billiard, which remain almost the same when varying the position of the inner circle induced by refractive index perturbation.

4. Conclusions

The observation of an all-optical induced transition from order to chaos in a silicon photonic system is of fundamental importance and offers new directions in applied research. Silicon photonics provides a rapidly growing platform for miniaturized optical devices. While currently its tool kit consists of traditional optical components, there is an increasing interest in developing functionality based on complex designs. Chaotic systems may offer new opportunities for controlling light on a chip, with potential applications in both passive and active environments including random bit generation [14], optical sensors, integrated spectrometers [38], and complex light sources [39]. The use of all-optical control to achieve a fundamental transition between integrable and non-integrable system is of interest for sensitively tuning these characteristics and achieving reconfigurable devices. While here we investigated the effect of wave chaos on statistics of classical light, application to quantum optical states will be of interest to explore new regimes of disorder-induced quantum coherence [40]. In conclusion, we demonstrated a transition from order to chaos in a photonic cavity through perturbation by an ultrafast pulsed laser. By employing ultrafast ultraviolet pump pulses we created refractive index perturbations based on plasma dispersion in a silicon photonic crystal cavity to induce chaos in the otherwise strictly classical cavity. Spatial mode maps obtained using ultrafast photomodulation reveal the spatial and spectral structure of the modes of the square cavity and allowed defining a spectrally integrated activity map of the system. For selected points we performed a quantitative analysis of the degree of chaos in the cavity based on spectral reconstruction, Δ_3 statistic, and random matrix theory. The statistical analysis demonstrated the quantum order-to-chaos transition. Comparison with random matrix

theory confirmed that the number of uncorrelated channels was reduced from more than 50 for the unperturbed cavity, to around two for the perturbed system. Our results show that ultrafast nano-optics provides new tools for studying quantum transport phenomena and grants access to the classical-to-chaos transition in complex systems.

5. Acknowldegment

ADF acknowledges support from EPSRC (EP/L017008/1). The research data supporting this publication can be accessed at http://dx.doi.org/10.17630/5857f38f-ee2b-494a-8e83-7529f1e6cebf.

Key words: Photonic crystals, instabilities and chaos, optical resonators, ultrafast processes in condensed matter, statistical optics.

References

[1] M. Sciamanna and K. Shore, Nature Photonics **9**(3), 151–162 (2015).
[2] L. Jackson, A. Lindgren, Y. Kim et al., IEEE Transactions on Circuits and Systems **31**, 1055 (1984).
[3] S. Alben and M. J. Shelley, Physical review letters **100**(7), 074301 (2008).
[4] V. Petrov, V. Gaspar, J. Masere, and K. Showalter, Nature **361**(6409), 240–243 (1993).
[5] S. J. Schiff, K. Jerger, D. H. Duong, T. Chang, M. L. Spano, W. L. Ditto et al., Nature **370**(6491), 615–620 (1994).
[6] L. Li, H. Peng, J. Kurths, Y. Yang, and H. J. Schellnhuber, Proceedings of the National Academy of Sciences **111**(23), 8392–8397 (2014).
[7] G. Demeter and L. Kramer, Physical Review Letters **83**(23), 4744 (1999).
[8] B. Xu, Y. C. Lai, L. Zhu, and Y. Do, Physical review letters **90**(16), 164101 (2003).
[9] I. Marginean, P. Nemes, and A. Vertes, Physical review letters **97**(6), 064502 (2006).
[10] A. E. Hramov, V. V. Makarov, A. A. Koronovskii, S. A. Kurkin, N. V. GaifullinM. B .and Alexeeva., K. N. Alekseev, M. T. Greenaway, T. M. Fromhold, A. Patane et al., Physical review letters **112**(11), 116603 (2014).
[11] D. Molenaar, H. Clercx, and G. van Heijst, Physical review letters **95**(10), 104503 (2005).
[12] C. Pirat, A. Naso, J. L. Meunier, P. Maïssa, and C. Mathis, Physical review letters **94**(13), 134502 (2005).
[13] A. Argyris, D. Syvridis, L. Larger, V. Annovazzi-Lodi, P. Colet, I. Fischer, J. García-Ojalvo, C. R. Mirasso, L. Pesquera, and K. A. Shore, Nature **438**(7066), 343–346 (2005).
[14] A. Uchida, K. Amano, M. Inoue, K. Hirano, S. Naito, H. Someya, I. Oowada, T. Kurashige, M. Shiki, S. Yoshimori et al., Nature Photonics **2**(12), 728–732 (2008).
[15] M. Olshanii, K. Jacobs, M. Rigol, V. Dunjko, H. Kennard, and V. A. Yurovsky, Nature communications **3**, 641 (2012).
[16] S. Perrard, M. Labousse, E. Fort, and Y. Couder, Physical review letters **113**(10), 104101 (2014).
[17] K. L. van der Molen, R. W. Tjerkstra, A. P. Mosk, and A. Lagendijk, Phys. Rev. Lett. **98**(Apr), 143901 (2007).
[18] C. Liu, A. Di Falco, D. Molinari, Y. Khan, B. Ooi, T. Krauss, and A. Fratalocchi, Nature Photonics **7**(6), 473–478 (2013).
[19] C. Liu, R. E. C. van der Wel, N. Rotenberg, L. Kuipers, T. Krauss, A. Di Falco, and A. Fratalocchi, Nature Physics (2015).
[20] C. Emary and T. Brandes, Physical Review E **67**(6), 066203 (2003).
[21] A. M. García-García and J. Wang, Physical review letters **94**(24), 244102 (2005).
[22] M. Santhanam and J. N. Bandyopadhyay, Physical review letters **95**(11), 114101 (2005).
[23] A. Relaño, Physical review letters **100**(22), 224101 (2008).
[24] F. S. Stephens, M. A. Deleplanque, I. Lee, A. O. Macchiavelli, D. Ward, P. Fallon, R. M. CromazM .and Clark., M. Descovich, R. M. Diamond et al., Physical review letters **94**(4), 042501 (2005).

[25] G. B. Lemos, R. M. Gomes, S. P. Walborn, P. H. S. Ribeiro, and F. Toscano, Nature communications **3** (2012).
[26] R. P. Taylor, R. Newbury, A. S. Sachrajda, Y. Feng, P. T. Coleridge, C. Dettmann, N. Zhu, H. Guo, A. Delage, P. J. Kelly, and Z. Wasilewski, Phys. Rev. Lett. **78**, 1952 (1997).
[27] A. Lagendijk, B. van Tiggelen, and D. S. Wiersma, Phys. Today **62**(8), 24–29 (2009).
[28] C. Liu, A. Di Falco, and A. Fratalocchi, Physical review X **4**(2), 021048 (2014).
[29] R. Bruck, B. Mills, B. Troia, D. J. Thomson, F. Y. Gardes, Y. Hu, G. Z. Mashanovich, V. M. Passaro, G. T. Reed, and O. L. Muskens, Nature Photonics **9**(1), 54–60 (2015).
[30] R. Bruck, B. Mills, D. J. Thomson, B. Troia, V. Passaro, G. Z. Mashanovich, G. T. Reed, and O. L. Muskens, Optics express **23**(9), 12468–12477 (2015).
[31] M. Abb, E. P. Bakkers, and O. L. Muskens, Phys. Rev. Lett. **106**(14), 143902 (2011).
[32] A. F. Koenderink, M. Kafesaki, B. C. Buchler, and V. Sandoghdar, Phys. Rev. Lett. **95**, 153904 (2005).
[33] J. Wang and A. G. Genack, Nature **471**, 345–348 (2011).
[34] S. Rotter, P. Ambichl, and F. Libisch, Phys. Rev. Lett. **106**, 120602 (2011).
[35] F. J. Dyson and M. L. Mehta, Journal of Mathematical Physics **4**(5), 701–712 (1963).
[36] A. Di Falco, T. Krauss, and A. Fratalocchi, Applied Physics Letters **100**(18), 184101 (2012).
[37] H. Weidenmüller and G. Mitchell, Reviews of Modern Physics **81**(2), 539 (2009).
[38] B. Redding, S. F. Liew, R. Sarma, and H. Cao, Nature Photonics **7**(9), 746–751 (2013).
[39] C. Conti and A. Fratalocchi, Nature Physics **4**(10), 794–798 (2008).
[40] H. E. Kondakci, A. F. Abouraddy, and B. E. A. Saleh, Nature Physics **11**, 930–935 (2015).